Appl. Phys. B 64, 49–56 (1997)

Applied Physics B Lasers and Optics

Investigation of two-wave mixing in arbitrary oriented sillenite crystals

E. Shamonina[1], G. Cedilnik[2], M. Mann[1], A. Kiessling[2], D. J. Webb[3], R. Kowarschik[2], K. H. Ringhofer[1]

[1] University of Osnabrück, Department of Physics, D-49069 Osnabrück, Germany
(Fax: + 49–541/969–2670, E-mail: ekaterina.shamonina@physik.uni-osnabrueck.de)
[2] Friedrich-Schiller-University Jena, Department of Physics, D-07743 Jena, Germany
[3] Applied Optics Group, Physics Laboratory, The University, Canterbury, Kent CT2 7NR, UK

Received: 19 March 1996/Accepted: 7 May 1996

Abstract. A generalized systematic description of the Two-Wave Mixing (TWM) process in sillenite crystals allowing for arbitrary orientation of the grating vector is presented. An analytical expression for the TWM gain is obtained for the special case of plane waves in a thin crystal ($|g|d \ll 1$) with large optical activity ($|g|/\varrho \ll 1$, g is the coupling constant, ϱ the rotatory power, d the crystal thickness). Using a two-dimensional formulation the scope of the nonlinear equations describing TWM can be extended to finite beams in arbitrary geometries and to any crystal parameters. Two promising applications of this formulation are proposed. The polarization dependence of the TWM gain is used for the flattening of Gaussian beam profiles without expanding them. The dependence of the TWM gain on the interaction length is used for the determination of the crystal orientation. Experiments carried out on $Bi_{12}GeO_{20}$ crystals of a non-standard cut are in good agreement with the results of modelling.

PACS: 42.40, 42.65, 42.70

Due to the inherent speed arising from their relatively short dielectric relaxation times and their wide availability, sillenite crystals like $Bi_{12}SiO_{20}$ (BSO), $Bi_{12}TiO_{20}$ (BTO) and $Bi_{12}GeO_{20}$ (BGO) are promising materials for real-time interferometry and image processing [1]. This explains the continuing interest of both experimentalists and theoreticians in photorefractive Two-Wave Mixing (TWM) in these crystals [2]. A correct description of the TWM process in sillenites is complicated by the presence of optical activity and linear birefringence induced by any applied electric field. The electro-optic tensor r_{ikl} responsible for the field-induced birefringence is described by T-symmetry [3]. The structure of the tensor r_{ikl} leads to the coupling of different components of the polarization vectors of two interacting waves. In addition, the coupling strongly depends on the orientation of the grating vector of the space-charge field with respect to the crystallographic axes. As a result, even in the idealized case of infinite plane waves intersecting at a small angle, a correct description of the polarization state involves two transverse components of the light field [4], and the evolution of the beams can only be modelled using a tensorial treatment of TWM.

Up to now, the majority of the published works have been devoted to a one-dimensional formulation, see e.g. [5–7]. In the special case of thin crystals with large optical activity, the analytical solution for the one-dimensional model [7] is sufficient to describe the TWM process. In the present article, we generalize the model presented in [7] to include an arbitrary orientation of the grating vector. However, in any real application, the interacting beams are unlikely to be planar and one must take into account their structure [8–10] and polarization properties [11] as well as the finite dimensions of the crystal [12, 13] and the crystal orientation [14].

A theoretical model including all these effects for the case of cylindrical symmetry was recently proposed [15]. The purpose of the present paper is to discuss the validity of both one-dimensional and two-dimensional models of real TWM experiments in sillenites. Most attention is paid to the influence of the grating vector orientation on the character of the energy exchange. It is also shown that a two-dimensional model allows the crystal to be easily characterized. The structure of this article is as follows. In Sect. 1, we obtain an analytical solution for the TWM gain with plane waves, allowing for an arbitrary grating vector orientation, and discuss the applicability of this one-dimensional model. In Sect. 2, the two-dimensional model of TWM with non-plane waves is reviewed and the expected new effects are qualitatively discussed. The results of numerical modelling in Sect. 3 confirm these theoretical expectations. As example applications of this theory, we describe a technique for flattening a Gaussian beam profile and a method for the determination of the crystal orientation. In Sect. 4, a comparison of the theory with experiments on unconventionally cut crystals[1] is carried out with good agreement.

[1] The normals of the faces of a "conventionally cut crystal" are pointing in the crystallographic directions [001], [110], [1$\bar{1}$0]

1 One-dimensional theory

In the optically isotropic sillenite crystals [3], the tensor of optical activity γ_{ikl} and the electro-optic tensor r_{ikl} have the form

$$\gamma_{ikl} = \gamma\varepsilon_{ikl}, \quad r_{ikl} = r|\varepsilon_{ikl}|,$$

where ε_{ikl} is the Levi-Civita symbol, $\rho = -2(\pi/\lambda)^2\gamma$ is the rotatory power, r is the effective electro-optic coefficient and λ is the wavelength.

We start with a simple idealization – the coupling of two plane waves $\mathbf{E}$ and $\mathbf{E}^{\mathrm{p}}$ in the diffusion regime. The interaction geometry, the crystal orientation and the coordinate system are shown in Fig. 1. We assume that the incident angles of both waves are small, so that the light rays inside the crystal propagate mainly in the $[1\bar{1}0]$ direction. Due to the small-angle approximation and the transversality of light waves [16] it is sufficient to consider only the x- and y-components of $\mathbf{E}$ and $\mathbf{E}^{\mathrm{p}}$, completely neglecting the z-component. Note that the grating vector of the space-charge field is located in the x–y plane having an inclination angle ξ with respect to the x-axis ($\xi = 0$ and $\xi = \pi/2$ correspond to the well-known longitudinal (L) and transverse (T) configurations, respectively). For simplicity, we do not consider refraction at the crystal boundaries and optical absorption. These physical factors will not influence such relative quantities as e.g. the gain (which will be defined later). The above simplifications lead to the following system of equations describing the photorefractive mixing of two plane waves in the steady state:

$$\frac{\partial\mathbf{E}}{\partial z} = \mathrm{i}\varrho\sigma_2\mathbf{E} + \mathrm{i}g^*\Sigma\mathbf{E}^{\mathrm{p}}, \tag{1a}$$

$$\frac{\partial\mathbf{E}^{\mathrm{p}}}{\partial z} = \mathrm{i}\varrho\sigma_2\mathbf{E}^{\mathrm{p}} + \mathrm{i}g\Sigma\mathbf{E}, \tag{1b}$$

with

$$\Sigma = \frac{1-\sigma_3}{2}\cos\xi + \sigma_1\sin\xi,$$

$$g = \mathrm{i}\Gamma\frac{m}{2},$$

$$\Gamma = \frac{\pi n^3 r}{\lambda}\frac{Kk_{\mathrm{B}}T/e}{1+(Kr_{\mathrm{D}})^2},$$

$$m = \frac{2\mathbf{E}^*\cdot\mathbf{E}^{\mathrm{p}}}{|\mathbf{E}|^2+|\mathbf{E}_0|^2}.$$

Here g is the coupling constant, Γ denotes the coupling coefficient, m the modulation of the interference pattern, σ_i the i-component of the vector of Pauli matrices, n the refractive index, and the asterisk complex conjugation. $r_{\mathrm{D}} = (\varepsilon_{\mathrm{st}}\varepsilon_0 k_{\mathrm{B}}T/N_{\mathrm{t}}e^2)^{1/2}$ is the Debye radius, $\varepsilon_{\mathrm{st}}\varepsilon_0$ the dielectric permittivity, k_{B} Boltzmann's constant, T the absolute temperature, e the electron charge, N_{t} the trap concentration and K the absolute value of the grating vector.

We are assuming that there is no applied external field and so we are operating in the diffusion regime. For crystals of BSO and BGO this further implies that $|g|/\varrho$ is small[2]. $|g|/\varrho$ will serve as a small parameter. Since there is no external field induced birefringence, the solution of (1a, b) is sought as a superposition of two circularly polarized eigenmodes of the optically active medium:

$$\mathbf{E} = E_+\mathbf{e}_+ + E_-\mathbf{e}_-, \quad \mathbf{e}_\pm = \frac{1}{\sqrt{2}}\begin{pmatrix}\pm 1\\ -\mathrm{i}\end{pmatrix}.$$

We define the gain, being a measure of the energy transfer between the pump and signal wave, as

$$G = \frac{|\mathbf{E}|^2 - |\mathbf{E}_0|^2}{|\mathbf{E}_0|^2}, \tag{2}$$

where $\mathbf{E}_0$ denotes the amplitude of the signal wave behind the crystal in the absence of the interaction with the grating. For sufficiently thin crystals[3] the system (1a, b) can be solved in first-order perturbation theory with the small parameter $|g|/\varrho$. For the gain, we obtain

$$G = \Gamma d\frac{\beta}{\beta+1}(\cos\xi\, f_\parallel + \sin\xi\, f_\perp), \tag{3}$$

with

$$f_\parallel = \cos(\varphi-\varphi^{\mathrm{p}})\left(\cos(\varphi-\varphi^{\mathrm{p}}) - \frac{\sin\varrho d}{\varrho d}\cos(\varphi+\varphi^{\mathrm{p}}-\varrho d)\right),$$

$$f_\perp = 2\cos(\varphi-\varphi^{\mathrm{p}})\frac{\sin\varrho d}{\varrho d}\sin(\varphi+\varphi^{\mathrm{p}}-\varrho d).$$

Here d is the crystal thickness, φ and φ^{p} are the initial polarization angles of the waves $\mathbf{E}$ and $\mathbf{E}^{\mathrm{p}}$ measured clockwise from the x-axis (we have assumed the incident states to be linearly polarized). $\beta = |\mathbf{E}^{\mathrm{p}}|^2/|\mathbf{E}|^2$ is the initial value of the beam ratio. The terms $f_\parallel$ and $f_\perp$ describe the contributions of the pure L- and pure T- components of the grating vector. With $\varphi = \varphi^{\mathrm{p}}$, $\xi = 0$ and $\xi = \pi/2$ we obtain the familiar formulae describing TWM in the L- and T-configurations, respectively (see [6, 7]).

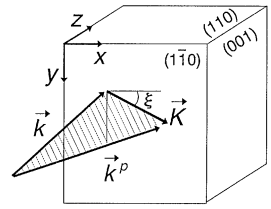

Fig. 1. Scheme of TWM with arbitrary oriented grating vector **K**

[2] The condition $|g|\varrho \ll 1$ is well fulfilled for BSO and BGO crystals in the absence of an external field, and it is invalid for BTO crystals even in the diffusion regime. For a typical experimental situation ($\lambda = 514.5$ nm, $Kr_{\mathrm{D}} = 1$) $|g|/\varrho \approx 0.09$–0.12 in BSO and BGO while $|g|/\varrho \approx 0.33$ in BTO

[3] The crystal is considered to be thin if the modulation depth m does not significantly change along the crystal depth, i.e. $|g|d \ll 1$. In the diffusion regime this is true at least for $d \ll 1.3$ cm (BSO, $\lambda = 514.5$ nm)

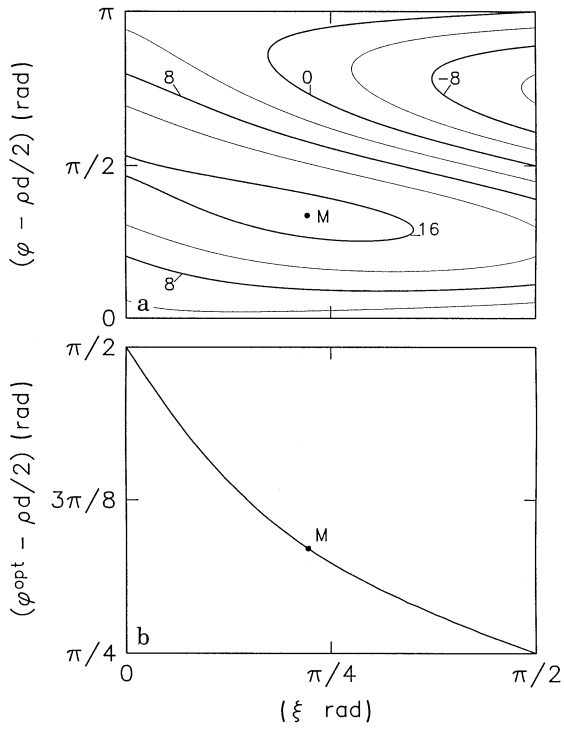

Fig. 2. **a** Dependence $(G\varphi, \xi)$; **b** dependence $\varphi^{opt}(\xi)$ for $\varrho d = \pi/2$. The remaining parameters are $n = 2.615$, $\varepsilon_{st} = 56$, $r = 5 \times 10^{-12}\,\mathrm{m\,V^{-1}}$, $N_t = 10^{22}\,\mathrm{m^{-3}}$, $\varrho = 36^\circ\,\mathrm{mm^{-1}}$, $Kr_D = 1$. The point M corresponds to the very maximum gain

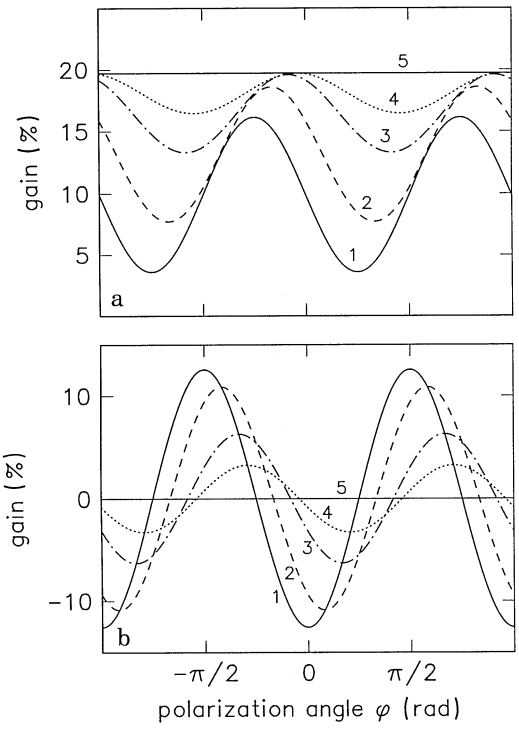

Fig. 3. Polarization dependence $G(\varphi)$ for **a** L- and **b** T-configurations for $\varrho d = \pi/2, 2\pi/3, 5\pi/6, 11\pi/12, \pi$ (curves 1–5, resp.). Note that curve 5 indicates the disappearance of the polarization dependence for $\varrho d = \pi$

In general, ξ can be arbitrary[4]. To the best of our knowledge, such a formula for the energy exchange, allowing the vector **K** to be arbitrarily oriented, is reported for the first time. Expression (3) permits us to analyze the influence of various factors (polarization of the waves, optical activity, crystal orientation and thickness) on the energy exchange in the TWM process. Such an analysis is of interest for a number of practical problems, e.g. for forward phase-conjugation schemes when two pairs of beams are in planes perpendicular to each other [14, 17, 18]. In the diffusion regime one cannot achieve very large gain. Therefore, the knowledge of optimum gain is of practical importance for real-time optical interferometry using sillenites. Unlike the T-configuration it is a characteristic feature of the L-configuration that the direction of the energy transfer does not change with increasing interaction length. In other words, in the L-configuration the amount of energy transferred from one beam to another will accumulate. As a result, for sufficiently thick crystals $[\sin(\varrho d)/\varrho d \ll 1]$ the maximum gain will always be achieved using the L-configuration. For thin crystals $[\sin(\varrho d)/\varrho d \leq 1]$, because of the competition between L- and T-contributions, the maximum gain can be achieved in a non-conventional configuration. An example of the dependence $G(\xi, \varphi)$ is presented in Fig. 2a, for the case $\varphi = \varphi^p$, $\varrho d = \pi/2$, $\beta = 1$. The parameters used correspond to a BSO crystal at $\lambda = 514.5$ nm [19]. It is seen that the optimum gain can be achieved neither for the L- nor for the T-configuration, but for an intermediate orientation of the grating vector (point M in Fig. 2).

For each grating orientation one can find the optimum polarization angle that leads to the highest local gain. Figure 2b presents the dependence of the optimum polarization angle on the grating orientation angle $\varphi^{opt}(\xi)$. It is seen that there is no linear dependence between φ^{opt} and ξ. A similar conclusion arising from numerical calculations has already been reported [14]. The authors of [14] have investigated the influence of external parameters (externally applied voltage and frequency detuning) on the optimum polarization angle and have found that the angle depends only on the direction of the grating vector. As $\varrho \to 0$, the dependence $\varphi^{opt}(\xi)$ becomes identical to that given in [14].

For certain particular values of ϱd, (3) cannot be used directly to determine the crystal orientation. This is easily understood, e.g. in the case $\varphi = \varphi^p$. The polarization dependence of the gain is most pronounced in the limiting case $\varrho d \to 0$, when the factor $\sin(\varrho d)/\varrho d \to 1$. At the same time, if $\varrho d \to \pi$, then $\sin(\varrho d)/\varrho d \to 0$, and the gain becomes independent of the initial direction of polarization. Figure 3a and b illustrates the influence of the parameter ϱd on the polarization dependence for the L- and T-configurations, respectively. We note that the situation $\varrho d \to \pi$ is realistic (for example, in a BSO crystal at a wavelength of 514.5 nm, $\varrho d \approx \pi$ for $d \approx 5$ mm). This

[4] Throughout this article, the phrase "arbitrary orientation of the grating vector" means that the grating vector still remains inside the x-y plane

means that for a wide class of parameters, it is difficult to observe a pronounced polarization dependence of the gain in experiments with plane waves. An alternative is to work with finite beams. A two-dimensional theory of TWM taking into account the transverse structure of the beams and the interaction geometry is presented in the next section.

2 Two-dimensional theory

2.1 General remarks

We consider a model based on the ideas of geometrical optics [15] and we restrict ourselves to an interaction geometry with invariance in one direction. In general, the interacting waves are not plane. Both the phase and amplitude of the waves may change over their cross-sections. Correspondingly, the coupling constant g can change over the beam cross-section as well as over the crystal depth. Furthermore, as a result of the overlap of two finite beams in a finite crystal, one has to deal with rather tedious boundary conditions. Remaining in the framework of the small-angle approximation, we get the following system of equations as a direct generalization of the system (1a, b):

$$(\mathbf{a}(\mathbf{r})\cdot\nabla)\,\mathbf{E}(\mathbf{r}) = \mathrm{i}\varrho\sigma_2\,\mathbf{E}(\mathbf{r}) + \mathrm{i}g^*(\mathbf{r})\,\Sigma\,\mathbf{E}^{\mathrm{p}}(\mathbf{r}) - \tfrac{1}{2}(\nabla\cdot\mathbf{a}(\mathbf{r}))\,\mathbf{E}(\mathbf{r}), \tag{4a}$$

$$(\mathbf{a}^{\mathrm{p}}(\mathbf{r})\cdot\nabla)\,\mathbf{E}^{\mathrm{p}}(\mathbf{r}) = \mathrm{i}\varrho\sigma_2\,\mathbf{E}^{\mathrm{p}}(\mathbf{r}) + \mathrm{i}g(\mathbf{r})\,\Sigma\,\mathbf{E}(\mathbf{r}) - \tfrac{1}{2}(\nabla\cdot\mathbf{a}^{\mathrm{p}}(\mathbf{r}))\,\mathbf{E}^{\mathrm{p}}(\mathbf{r}). \tag{4b}$$

$\mathbf{a}^{\mathrm{p}}$ and $\mathbf{a}$ are the spatially dependent unit vectors determining the propagation direction of the different rays of the pump and signal waves, respectively, and define the interaction plane. Equations (4) describe a rather general case of the evolution of the amplitudes of optical waves during their propagation through an optically active crystal with an arbitrary refractive-index grating. The terms containing $\nabla\cdot\mathbf{a}^{\mathrm{p}}$ and $\nabla\cdot\mathbf{a}$ on the right-hand side of the system (4a, b) are new. They vanish when the pump and signal waves are plane. As before, the interaction plane is inclined at an angle ξ with respect to the x–z plane (see Fig. 1, vector **K**). We introduce a new coordinate w, so that the interaction plane will be the w–z plane. The interaction geometry of two finite waves is shown in Fig. 4. For the signal wave, we distinguish regions 1–3 where different terms on the right-hand side of (4a) are non-zero. Inside the crystal, the light waves interact in region 1 (all terms contribute). In region 2, the waves do not interact ($g = 0$). Outside the crystal (region 3), only the term with $\nabla\cdot\mathbf{a}$ remains. For the pump wave, there are analogous regions.

2.2 Qualitative discussion

The interaction geometry presented in Fig. 4 is just a particular case. In general, two beams of arbitrary shape may overlap within a crystal in many different ways. Consequently, the system (4a, b) can in general be solved only numerically. Contrary to the assumptions necessary for obtaining the analytical solution of the one-dimensional

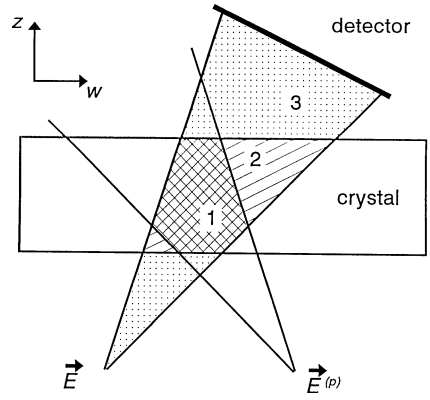

Fig. 4. Interaction geometry of two finite beams in a crystal

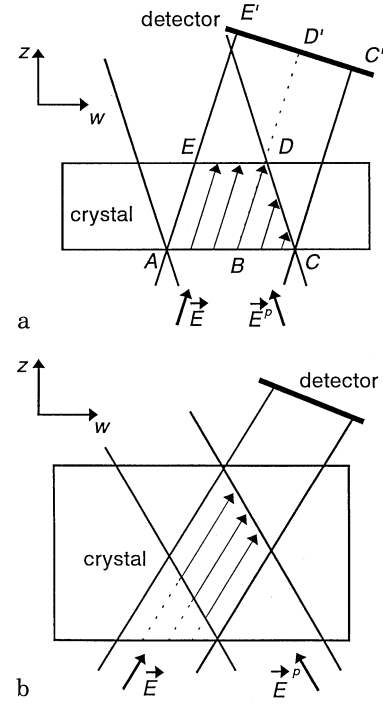

Fig. 5. Two plane beams in **a** a trapezoid and **b** a rhombus geometry

case, there will be no restriction on the parameters $|g|d$ and $|g|/\varrho$. System (4a, b) yields the vector amplitudes of the signal wave in regions 1–3 (Fig. 4), before and after the interaction with the pump wave.

In experiments, it is of course generally only possible to measure the intensity outside the crystal. However, the following two subsections show how it is possible to study the energy exchange inside the crystal with the help of intensity measurements at a detector located behind the crystal. We propose to use two geometrical arrangements that we call the "trapezoid" and "rhombus" geometries (Fig. 5a and b, respectively). These notations are clear from the figure.

2.2.1 *Trapezoid geometry*. The arrows in Fig. 5a show schematically the interaction paths for different rays of the

signal wave. It is seen that for one part of the signal beam (the quadrangle $ABDE$) all the rays interact with the pump wave over the entire crystal. In the other part of the signal beam (the triangle BCD), the interaction length is different for each ray. It falls down from its maximum value to zero as one moves along the crystal face from B to C. Consequently, we expect that the signal beam will behave differently at the detector in the regions $E'D'$ and $D'C'$. The initial polarization state of the signal wave at the crystal front face remains unchanged over the beam cross-section. If the intensity profiles of both waves are plane, each ray of the signal wave in the region $ABDE$ will have both equal interaction lengths and boundary conditions. As a result, assuming a perfect crystal, one can expect the same changes of intensity for all these rays, i.e. a constant distribution of the gain in the interval $E'D'$ will be observed. At the same time, the change of the gain in the detector interval $D'C'$, corresponding to the region BCD, will be determined by the change in the interaction length. The gain changes from its value obtained at the maximal interaction length (point D') to zero (absence of interaction, point C'). Let us emphasize that, since the interaction length changes through the beam cross-section, the problems connected with $\varrho d \approx \pi$ can be avoided.

2.2.2 *Rhombus geometry*. In the rhombus geometry (Fig. 5b), both beams overlap completely inside the crystal. In the case of different widths of pump and signal wave, the interaction region is a parallelogram rather than a rhombus. In contrast to the previous case, all rays of the signal wave interact with the pump wave over the same distance (as indicated by arrows). However, before entering the interaction region, the rays of the signal wave follow different optical paths inside the crystal (denoted by dotted lines). Due to optical activity, each ray of the signal beam has a different polarization state at the entrance of the interaction region. That is, the amplitude of the signal wave will be polarization-modulated. Consequently, the dependence of the gain on the detector coordinate corresponds to the polarization dependence of the gain. Note that, in this geometry, the interaction length depends on the width of the interacting beams rather than on the crystal thickness. One can always avoid problems connected with $\varrho d \approx \pi$ by, e.g., varying the width of the pump wave. Moreover, in order to obtain the polarization dependence of the gain by means of the conventional one-dimensional method, one has to carry out a set of measurements with different initial polarizations of the beams. Using the two-dimensional rhombus geometry, one is able to get the polarization dependence in a single measurement. Obviously, the rhombus geometry is reasonable only for sufficiently large values of the optical activity (BSO, BGO) and crystal thicknesses.

3 Numerical results

All numerical simulations in two dimensions are performed using a program package described in detail in [20]. The procedure is based on the method of characteristics [21].

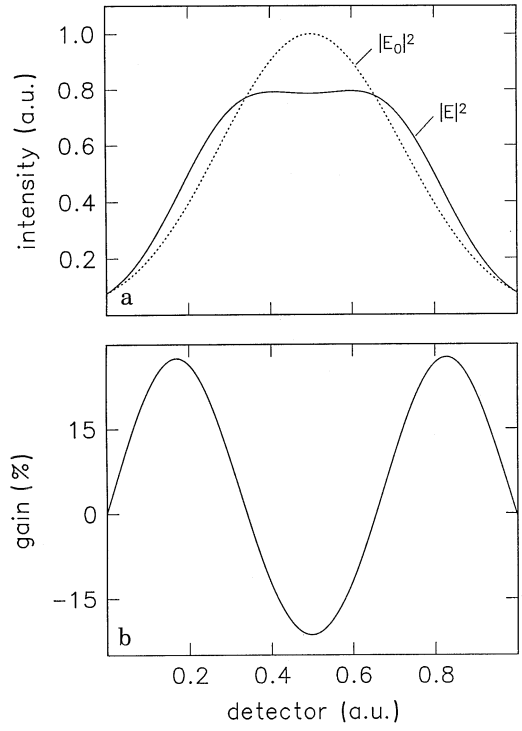

Fig. 6. Flattening of the Gaussian beam: **a** signal intensity and **b** gain at the detector (rhombus geometry)

3.1 Flattening Gaussian beam profiles

In this subsection we use the rhombus geometry for shaping signal intensity profiles which can be of great importance for, e.g., laser projection printing, material characterization, etc. [22]. We consider the interaction of two plane waves with Gaussian intensity profiles in the T-configuration. Both waves are initially equally polarized ($\varphi = \varphi^{\mathrm{p}} = 3\pi/4$). The beam ratio $\beta = 100$. The interaction lengths correspond to $\varrho l = \pi/2$ for the signal wave and $\varrho l = 3\pi/2$ for the pump wave. The remaining parameters are the same as in Fig. 2. Figure 6a presents the intensity profile of the signal wave at the detector before and after the interaction with the pump wave. One can see that the initial Gaussian profile has been flattened. The corresponding dependence of the gain at the detector is shown in Fig. 6b. Due to the continuously varying initial polarization at the boundary of the interaction region, the central part of the signal wave is depleted whereas the sides of the signal wave gain energy. As a result, one is able to flatten the incoming Gaussian profile without changing its phase (i.e. without expanding it). As is well known [22], there is a necessity for illuminating an object field with a uniform intensity distribution without expanding the laser beam. We believe that the proposed method can be easily applied to a practical flattening of Gaussian profiles using BSO (or BGO) crystals of sufficient thickness.

3.2 Influence of the crystal orientation on the energy exchange

Now we consider the trapezoid geometry and allow for an arbitrary orientation of the grating vector. The limiting

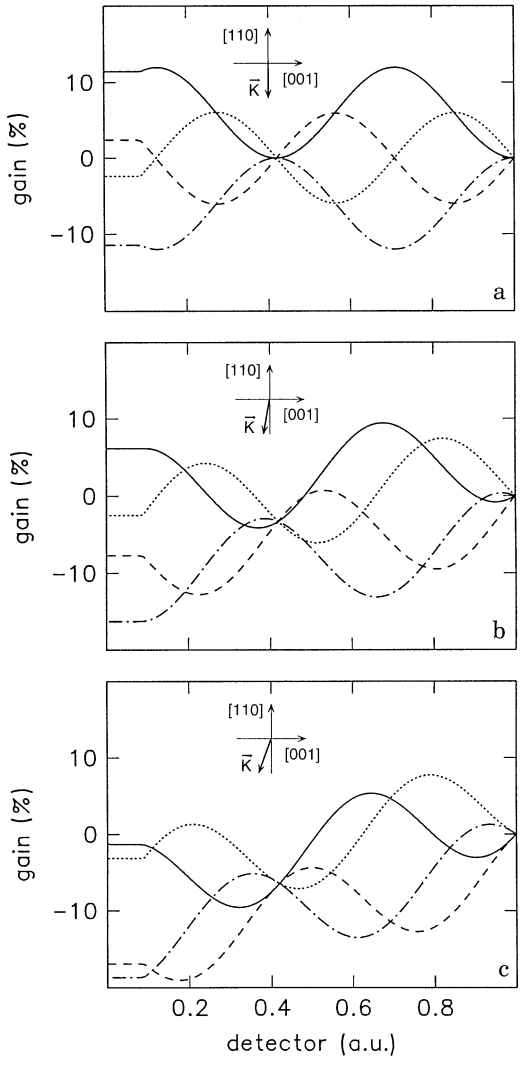

Fig. 7. Influence of the grating vector orientation on the TWM. Gain at the detector for $\xi = 90°$ **a**, 100° **b**, 110° **c** (trapezoid geometry). The initial polarization corresponds to $(\varphi - \xi) = 0$ (solid), $\pi/4$ (dashed), $\pi/2$ (dashed-dotted), $3\pi/4$ (dotted line)

cases are the L- and T-configurations. In order to change from the first to the second configuration, one can rotate either the grating vector or the crystal by $\pi/2$ about the propagation axis of the crystal ($[1\bar{1}0]$). Intermediate configuration where the grating vector is inclined at an arbitrary angle ξ to the axis [001] can be realized e.g. in forward phase-conjugation processes [17]. Such a situation can also occur in ordinary TWM experiments, for example, if the crystal is cut in such a way that its surfaces are not exactly parallel to the planes (001), (110) and ($1\bar{1}0$). In this case, it would be useful for experimentalists to be able to determine the real crystal orientation through some simple TWM experiments. Therefore, it is worth studying the influence of the crystal orientation on the TWM process.

In Fig. 7 the dependence of the gain on the detector coordinate is shown for various grating vector orientations. The crystal thickness corresponds to $\varrho d = 3\pi/2$, the beam ratio is $\beta = 1$ and the remaining parameters are as in Fig. 2. Figure 7a is for the T-configuration and different initial polarizations (see the figure caption). Figures 7b and c are for slightly different crystal orientations. As discussed above, Fig. 7 can be interpreted as the dependence of the gain on the interaction length. The plateaus at the left side are due to equal boundary conditions and interaction lengths (interval $E'D$ in Fig. 5a). As can be seen from the figure, slight changes of the orientation of the grating vector lead to perceptible changes in the gain distribution at the detector. In the T-configuration, by changing the polarization state, it is possible to change the direction of the energy transfer between the pump wave and the signal wave. In the case $\beta = 1$, the theoretical gain distributions with the chosen initial polarizations are symmetric with respect to the direction of the energy transfer (Fig. 7a). With increasing deviation from the T-configuration, this symmetry is gradually destroyed (Fig. 7b, c). This is because the real configuration is a mixture of the L- and T-configurations. By deviating from the T-configuration naturally the longitudinal part of the configuration increases and the direction of the energy transfer in the L-configuration prevails. Using such a measurement on a crystal with unknown surface normals, it is possible to calculate the deviation of the grating vector from the T- or L-case, as will be shown in the following section.

4 Experimental results

We have investigated a set of BGO crystals of different thicknesses (from 2 to 8 mm). The input face of all the crystals was the same – $(1\,\bar{1}\,0)$. We have chosen this set of crystals (all from the same manufacturer) since in conventional one-dimensional measurements, using what was believed to be the L- and T-configurations, the dependence of their gain on their input polarization state demonstrated an unexpected behavior. Furthermore, because of their different thicknesses, the investigation of the polarization dependence with the one-dimensional method for plane waves was not equally successful for all crystals. Therefore, we used finite beams to clarify the true crystal orientations.

The experimental arrangement is shown schematically in Fig. 8. The plane wave from the Ar^+ laser ($\lambda = 514.5$ nm) is split into the Signal Wave (SW) and Pump Wave (PW) by a Polarizing Beam Splitter (PBS). The beam ratio is $\beta \approx 40$ and the pump intensity is 80 $W\,m^{-2}$. A polarizer (P) is inserted to improve the polarization purity of the signal wave. The half-angle between the symmetrically incident beams is 23°. With the Half-Wave Plates (HWP1, HWP2) the polarization angle φ of both waves can be chosen. The slit S of width 3 mm in front of the crystal (polished surface) cuts both beams; the overlap inside the crystal corresponds to the trapezoid geometry, see Fig. 5a. The lens L behind the crystal transmits the image of the signal wave in the neighborhood of the slit's edge on a CCD camera. The digitized two-dimensional image with 512×512 pixels is spatially averaged over the vertical coordinate of the detector in order to obtain a one-dimensional intensity distribution at the detector line.

As an example, we discuss here the results obtained for the crystal with $d = 8$ mm. We denote as the L'-config-

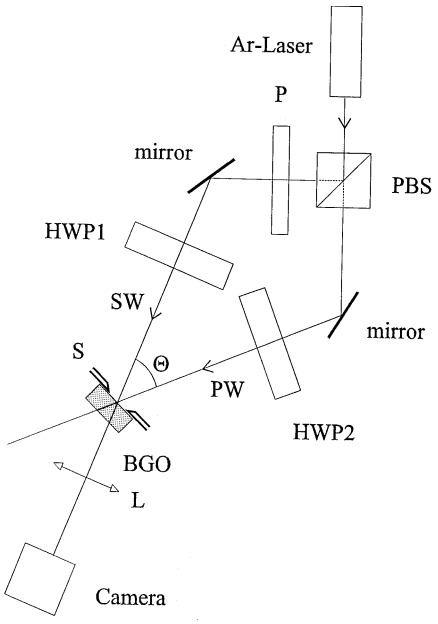

Fig. 8. Experimental setup for TWM. Due to the slit S in front of the BGO crystal, the interaction region inside the crystal is a trapezoid

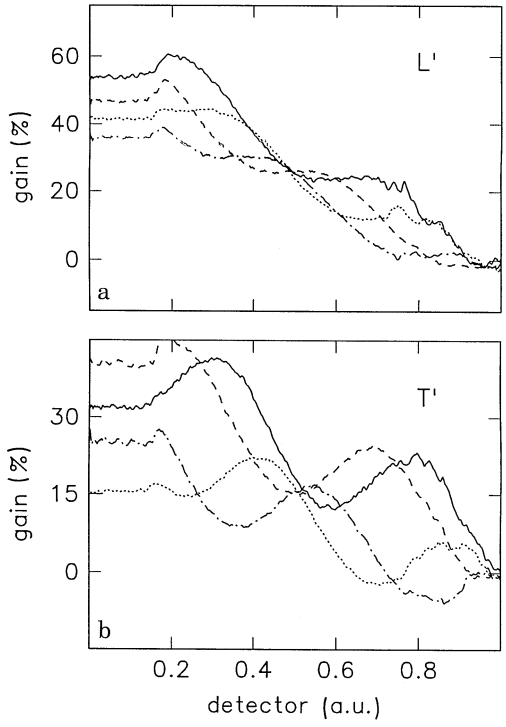

Fig. 9. Measured gain at the detector in **a** the L'-configuration and **b** the T'-configuration. The initial polarization corresponds to $(\varphi - \xi) = 0$ (solid), $\pi/4$ (dashed), $\pi/2$ (dashed-dotted), $3\pi/4$ (dotted line)

uration the case with the grating vector perpendicular to one unpolished surface, and as the T'-configuration the case (perpendicular to the first) with the grating vector perpendicular to another unpolished surface. Figure 9a and b shows the measured gain at the detector for the L'-

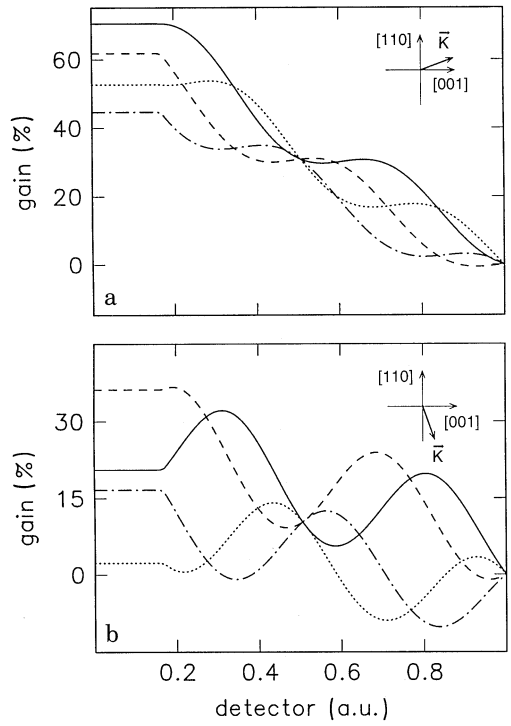

Fig. 10. Calculated gain at the detector for L' **a** and T' **b** configurations. The initial polarization corresponds to $(\varphi - \xi) = 0$ (solid), $\pi/4$ (dashed), $\pi/2$ (dashed-dotted), $3\pi/4$ (dotted line)

and T'-configurations, respectively. The different curves correspond to different initial polarizations of the incident beams (see the figure caption). Using standard parameters for BGO crystals [19], we have modelled this experiment numerically, allowing for an arbitrary orientation of the grating vector and fixing all other parameters. The results are presented in Fig. 10a and b for the L'- and T'-configurations, respectively. Because of various experimental influences (like light reflection at crystal surfaces, leading to multiple wave coupling[5], crystal inhomogeneities, and so on), it is of little use to make a quantitative comparison of experimental and numerical results. Visually, the best agreement is achieved for $\xi = 340°$ in the L'-configuration and for $\xi = 70°$ in the T' configuration. Thus, we get in both cases the same deviation of 20° from the correct L- and T-configurations. We concluded that in this crystal both unpolished surfaces were in error by angles of 20° with respect to the conventional cut assumed at the beginning.

To check the alignment of the faces of the crystal, X-ray techniques were used. These showed that the polished surfaces of the crystal $(1\bar{1}0)$ were cut correctly, and the other faces were in error by angles $(17 \pm 1)°$. This

[5] At the detector (point D' in Fig. 5a), a step is observed in the gain curve. It appears in both the L'- and T'-configurations for any polarization in the vicinity of the detector coordinate 0.2 (see Fig. 9). We believe that this is because of the reflection of the pump wave between D and E (Fig. 5a) into the direction opposite to the signal wave from the backface of the crystal. As a result, the conditions for the interaction in the corresponding region of the crystal ($ABDE$) change, which in turn manifests itself in the step in the gain curve

result is in good agreement with that obtained with finite beam measurements. Analogous investigations with other crystals of this set lead to similar success in determining the correct crystal orientation. The values for ξ obtained with X-ray techniques and with our method differ by less than (3–4)°. One cannot expect a better agreement for intensity measurements. Nevertheless, using simple TWM experiments with finite beams, one can easily and with good accuracy get information about crystal orientation. Since the equipment for X-ray diffraction is not available in many optical laboratories, we believe that the proposed method may be useful for the characterization of optically active crystals.

5 Conclusions

For the case of thin crystals with large optical activity, we obtained an analytical expression for the TWM gain of plane waves allowing for an arbitrary orientation of the grating vector. In the case $\varrho d = \pi$ the polarization dependence of plane waves vanishes. Alternatively, a two-dimensional approach can be used. It permits the determination of the polarization- and thickness-dependences of the TWM gain by an analysis of the deformation of the intensity profiles of finite beams. We point out the possibility of using this approach for flattening Gaussian beam profiles without expanding them and for determining the crystal orientation.

Experiments with finite beams and with BGO crystals of a non-standard cut have been performed with the aim of determining the crystal orientation. The results agree well with the results obtained by X-ray diffraction.

Acknowledgements. We would like to thank the Deutsche Forschungsgemeinschaft for financial support within the Sonderforschungsbereich 225. We also thank H. Hesse for the X-ray measurements and helpful discussions, and M. Shamonin for a critical reading of the manuscript. D. J. W. would also like to thank the DAAD for support.

References

1. M.P. Georges, P.L. Lemaire: Appl. Opt. **34**, 7497 (1995)
2. Technical Digest on Photorefractive Materials, Effects and Devices II (Aspen, USA 1995)
3. A. Yariv, P. Yeh: Optical Waves in Crystals, Wiley Series in Pure and Applied optics (Wiley, New York 1984) pp. 223–237
4. H.C. Pedersen, P.M.B. Johansen: Pure Appl. Opt. **2**, 659 (1993)
5. A. Marrakchi, R.V. Johnson, J.A.R. Tanguay: J. Opt. Soc. Am. B **3**, 321 (1986)
6. S. Mallick, D. Rouède, A.G. Apostolidis: J. Opt. Soc. Am. B **4**, 1247 (1987)
7. D.J. Webb, A. Kiessling, B.I. Sturman, E. Shamonina, K.H. Ringhofer: Opt. Commun. **108**, 31 (1994)
8. L. Solymar, D.J. Cooke: Volume Holography and Volume Gratings (Academic Press, London 1981) pp. 164–207
9. L. Boutsikaris, F. Davidson: Appl. Opt. **32**, 1559 (1993)
10. D. Fluck, S. Brülisauer, P. Günter: Opt. Commun. **115**, 626 (1995)
11. A. Brignon, K.H. Wagner: Opt. Commun. **101**, 239 (1993)
12. G. Notni, R. Kowarschik: J. Opt. Soc. Am. A **11**, 1682 (1989)
13. W. Królikowski, M. Cronin-Golomb: Opt. Commun. **89**, 88 (1992)
14. H.C. Ellin, M.V. Shamonin, L. Solymar: Int. J. Opt. Comput. **2**, 239 (1991)
15. E. Shamonina, M. Mann, K.H. Ringhofer, A. Kiessling, R. Kowarschik: Opt. Quant. Electron. **28**, 25 (1996)
16. K.H. Ringhofer, S. Tao, J. Takacs, L. Solymar: Appl. Phys. B **52**, 259 (1991)
17. A. Khyzniak, V. Kondilenko, Yu. Kucherov, S. Lesnik, S. Odulov, M.S. Soskin: J. Opt. Soc. Am. A **1**, 169 (1984)
18. J. Takacs, H.C. Ellin, L. Solymar: Opt. Commun. **93**, 223 (1992)
19. M.P. Petrov, S.I. Stepanov, A.V. Khomenko: Photorefractive Crystals in Coherent Optical Systems, Springer Series in Optical Sciences (Springer, Heidelberg 1991) pp. 233–239
20. M. Mann, E. Shamonina, K.H. Ringhofer: Modelling of two-wave mixing experiments in sillenite crystals, Comp. Phys. Commun., accepted for publication (1996)
21. W.F. Ames: Numerical Methods for Partial Differential Equations (Academic Press, New York 1977) pp. 165–193
22. S. Jamet, C. Ötzkul: Opt. Commun. **110**, 651 (1994)